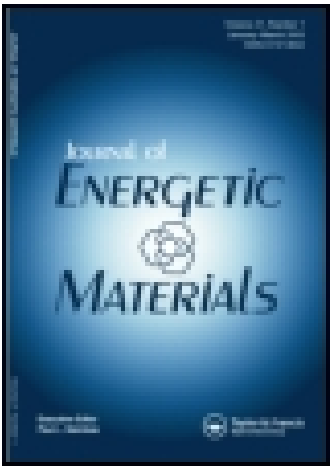

Journal of Energetic Materials

Publication details, including instructions for authors and subscription information:
http://www.tandfonline.com/loi/uegm20

Preparation and explosive properties of azo- and azoxy-furazans

David Chavez [a], Larry Hill [a], Micheal Hiskey [a] & Scott Kinkead [a]

[a] Los Alamos National Laboratory DX-2, High-Explosives Science and Technology, MS C920, Los Alamos, NM, 87545, USA

Published online: 20 Aug 2006.

To cite this article: David Chavez, Larry Hill, Micheal Hiskey & Scott Kinkead (2000) Preparation and explosive properties of azo- and azoxy-furazans, Journal of Energetic Materials, 18:2-3, 219-236, DOI: 10.1080/07370650008216121

To link to this article: http://dx.doi.org/10.1080/07370650008216121

PREPARATION AND EXPLOSIVE PROPERTIES OF AZO- AND AZOXY-FURAZANS

David Chavez, Larry Hill, Michael Hiskey* and Scott Kinkead
Los Alamos National Laboratory
DX-2, High-Explosives Science and Technology, MS C920
Los Alamos NM 87545 USA

ABSTRACT

The synthesis and properties of three energetic azo- and azoxyfurazans are described. All are derived from oxidation of 3,4-diaminofurazan (DAF) (**1**) and include 3,3'-diamino-4,4'-azoxyfurazan (DAAF) (**2**), 3,3'-diamino-4,4'-azofurazan (DAAzF) (**3**) and bis[1,2,5]oxadiazolo[3,4-c:3',4'-g][1,2,5,6]tetrazocine (DFT) (**4**). The explosive performance properties of DAAF and DAAzF have been investigated.

INTRODUCTION

The synthesis of 3,4-diaminofurazan (**1**) was first reported in 1968 in an article from this laboratory.[1] Since then a large body of work has been accumulated on the oxidation of (**1**), especially by Russian scientists.[2-6] We became interested in these compounds as they represent a unique class of energetic materials. Compounds (**2**)-(**4**) (FIGURE 1) derive a significant amount of their energy of detonation from their intrinsically high heats of formation (ΔH_f) and not from oxidation of carbon in the backbone. This, in a large part, is due to the presence of the azo- and azoxy- linkage. As an example of this, compound (**3**)

Journal of Energetic Materials Vol. 18, 219-236 (2000)
Published in 2000 by Dowden, Brodman & Devine, Inc.

FIGURE 1
Oxidation Products of 3,4-Diaminofurazan (1)

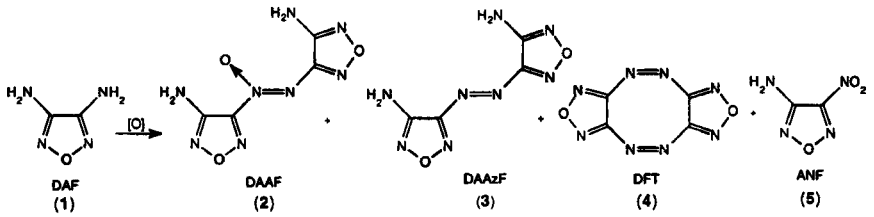

only has enough available oxygen to burn its hydrogen to water and none to oxidize carbon, yet it has better explosive performance than HNS (2,2',4,4',6,6'-hexanitrostilbene) which is able to burn 64% of its carbon to CO (FIGURE 2). In addition the impact sensitivity of (3) was determined to be greater than 320 cm while the drop height of HNS was published to be 54 cm (2.5 kg, Type 12).[7]

FIGURE 2
Comparison of Detonation Stoichiometry and Performance of HNS to DAAzF (3)

$C_4H_4N_8O_2 \rightarrow 2\ H_2O + 4\ N_2 + 4\ C$	V_D=7.42 km/s at 1.60 g/cm^3
DAAzF (3)	P_{CJ}=262 kbar at 1.65 g/cm^3
$C_{14}H_6N_6O_{12} \rightarrow 3\ H_2O + 3\ N_2 + 9\ CO + 5\ C$	V_D=6.80 km/s at 1.60 g/cm^3
HNS	P_{CJ}=200 kbar at 1.60 g/cm^3

RESULTS

The first preparation of 3,3'-diamino-4,4'-azoxyfurazan (DAAF) (2) to appear in the literature was in 1981 by Russian scientists.[2] They used a variety of peroxide reagents on 3,4-diaminofurazan (1) to prepare (2), (3) and 3-amino-4-nitrofurazan (5), usually as mixtures which were separated by their differing solubilities. We found the room temperature oxidation of

diaminofurazan (1) utilizing sulfuric acid and hydrogen peroxide to be the most convenient method, giving 88% crude yields of (2) containing a few percent of amino-nitrofurazan (5). The (5) present in this mixture severely depresses the DSC onset temperature. Fortunately this contaminant was easily removed by a single recrystallization from DMSO/H_2O. Pure DAAF (2) is an orange-yellow crystalline powder having a DSC onset of 248°C and an x-ray crystal density of 1.747 g/cm^3.[8] Scanning electron microscopy (SEM) on the powder revealed it to be stacks of jumbled cubes. The ΔH_f was measured at +106 kcal/mol by combustion calorimetry. DAAF (2) has a drop height of greater than 320 cm (2.5 kg, Type 12) and elicits no response to spark (>0.36 J) or friction (>36 kg, BAM). Low density pellets of DAAF can be pressed neat but high density pellets tend to wafer and therefore required formulation with 5 volume percent of latex Kel-F 800. This allowed pressing of pieces up to a density of 1.70 g/cm^3 (97% of theoretical maximum density). A Henkin critical temperature was determined to be 241°C for the Kel-F formulated material and 252°C for the neat material.

The explosive performance properties of DAAF (2) proved to be interesting. A poly-ρ test, which determines detonation velocity as a function of density, was performed at two diameters, 0.5 in. and 0.25 in. These two diameters revealed that the detonation velocity was relatively independent of diameter as shown in FIGURE 3. This data was further verified by an unconfined rate stick of pellets at a density of 1.69 g/cm^3 and 3 mm in diameter. As evidenced by the witness plate a complete detonation was

FIGURE 3
Detonation Velocity as a Function of Density at 0.5 in. and 0.25 in. for DAAF (2) + 5 vol.% Kel- F 800

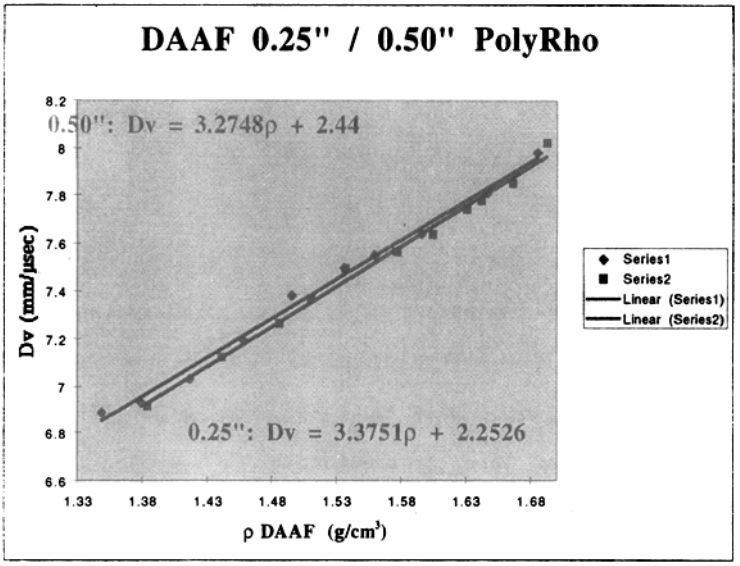

achieved. Unfortunately this test was too small to be instrumented accurately to determine detonation velocity. A failure diameter of less than 3 mm is unprecedented in a material which is insensitive to impact. The detonation pressure (P_{CJ}) was estimated to be 299 kbar from a 0.5 in. diameter plate dent at a density of 1.69 g/cm^3.

Shock sensitivity was characterized by performing six wedge tests, in which the DAAF was plastic-bonded with 5% Kel-F and pressed to 1.705 g/cm^3. There have been many variations on the wedge test; the present one is the so-called "mini-wedge" test[9,10] which is designed to use a minimal amount (about 7 g) of sample explosive. Material conservation is desirable for screening new explosives, as their manufacture tends to be costly.

The wedge test begins by generating a plane detonation via an explosive plane wave lens. The detonation emerging from the lens initiates a pad of booster explosive, and the detonation emerging from the booster explosive drives a shock wave through one or more layers of inert attenuator plates. These alter the transmitted pressure via wave reflections. Thus, the test pressure is controlled by choosing the booster explosive, the number of attenuator plates, and their materials. (The "stack-ups" for each experiment and the corresponding results are listed in Table 1.) Note that the shock is intended to be "supported", meaning that the pressure remains constant after the passage of the shock front; but in reality the pressure decays slightly due to the Taylor wave in the driving explosive.

TABLE 1
Wedge Test Parameters

		Shot Number					
	Unit	15-2758	15-2760	15-2759	15-2757	15-2756	15-2752
Booster HE		2" Baratol	2" Baratol	2" Baratol	2" Baratol	2" Baratol	2" TNT
Attentuator plate #1		0.75" Brass	0.75" Brass	.50" PMMA	1" SS	2" Alum.	2" Alum.
Attentuator plate #2		.5" PMMA	.5" Teflon	.75" SS	1" Alum.	none	none
Attentuator plate #3		.63" Alum	.63" Alum	.63" Alum	none	none	none
Initial Particle Velocity	mm/μs	.58	.62	.81	.85	1.07	1.27
Initial Shock Velocity	mm/μs	3.5	3.72	3.98	4.04	4.18	4.94
Input Pressure	GPa	3.46	3.88	5.49	5.87	7.87	10.5
Run to Detonation	mm	No tran	10.9	4.64	3.4	1.87	1.39
Time to Detonation	μs	No tran	2.96	1.17	.084	.39	.19

The wedge-shaped explosive sample is mounted to the final attenuator plate, from which it receives the transmitted shock wave. The progress of the wave is observed by tracking its intersection with the wedge face. This intersection is characterized by a prompt decrease in surface reflectivity, which is observed by illuminating the sample with an argon flash and photographing the wedge face with a streak camera. Provided that the wedge angle is sufficiently small (in this case 30°), the progress of the shock is unaffected by the presence of the free surface. The reader is referred to ref. 10 for more details about the mini-wedge test configuration.

A sufficiently strong shock will initiate a degree of reaction that causes the wave to accelerate, ultimately to a steady detonation. The shorter the run distance to detonation for a given input pressure, the more shock-sensitive the explosive. It is customary to plot the run distance (or time) to detonation versus input shock pressure, the so-called "Pop-plot". Experience has shown that over the range of input pressures typically measured, the resulting curves follow a power law.

The distance and time to detonation can be read directly from the film record, subject to a chosen criterion for defining the transition point. Unfortunately this criterion varies from author to author; fortunately, it is somewhat forgiving because the wave accelerates extremely rapidly near transition. Here, we define transition as the point at which the wave speed departs from the straight line associated with the ultimate detonation velocity, as read directly from the film record.

The input pressure attained in the explosive is inferred from impedance matching. This calculation uses 1) the measured initial shock velocity from the film record, 2) the measured initial free-surface velocity of the base plate to which the sample is mounted, 3) the known shock properties and density of this plate, and 4) the initial explosive sample density.

A power law fit to the six Pop-plot points gives the equation:

$$\log[x^*] = 2.21 - 2.10\log[P] \qquad (1)$$

with pressure in Gigapascals and run distance in millimeters. This curve fit and data points are plotted in FIGURE 4, together with curves for neat-pressed PETN,[11] PBX 9501 (95 wt% HMX, 5 wt% binder),[11] and PBX 9502 (95 wt% TATB, 5 wt% binder).[12] It is clear that DAAF is quite like HMX so far as shock-sensitivity is concerned. The degree of scatter in the points is typical of a plane-wave driven wedge test; here the biggest errors are believed to be limited planarity and pressure support of the input shock.

The analysis that yields input pressure also gives the initial material velocity u_p in the explosive. These values, correlated with the initial shock velocity u_s, define the inert Hugoniot (the locus of final shocked states given an initial state) for the explosive. We may take the explosive to be inert at early times at which material has had essentially no time to react. Often the "u_s-u_p" Hugoniot is linear, or nearly so, in the range measured. In this case the best linear fit is:

$$u_s = 2.51 + 1.79u_p \qquad (2)$$

FIGURE 4
Run Distance to Detonation vs. Input Pressure (Pop Plot) for DAAF, Together With Curves for PETN, PBX 9501 and PBX 9502.

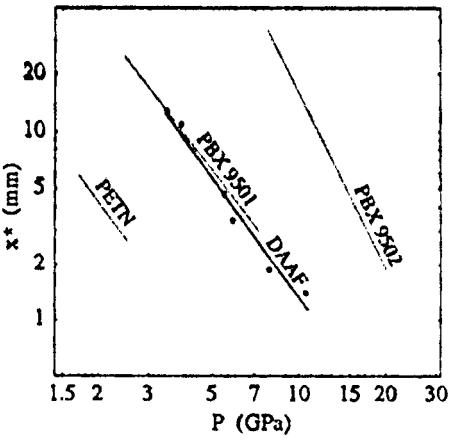

with u_s and u_p in mm/μs. Equation (2) and the corresponding data points are plotted in FIGURE 5, together with fits to data for PETN, PBX 9501 and PBX 9502, the same sets of experiments as shown in FIGURE 4. Note that, unlike the Pop-plot, the Hugoniot curves for solid explosives tend to be quite similar to one another, reflecting the fact that their mechanical properties tend to be similar. Note also that some explosives, in this example PBX 9502, have markedly nonlinear Hugoniot curves.

The explosive energy was characterized by performing a standard 1-inch cylinder test on DAAF/5 vol.% Kel-F 800 pressed to 1.691 g/cm^3. The test consists of a 1.00-inch inner diameter, 0.10-inch wall copper tube filled with explosive and detonated at one end. The pressure of the explosive products expands the tube in a funnel shape. With the proper care the tube will typically expand to about three times its initial diameter before it begins

FIGURE 5
Inert Hugoniot for DAAF, Together With Curves for PETN, PBX 9501, and PBX 9502

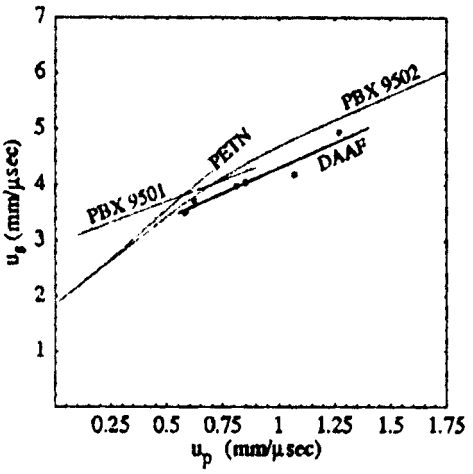

to fragment. To achieve this much expansion requires very tight mechanical tolerances and high standards of purity, temper, and grain size for the copper. These requirements are laid out in more detail in ref. 13.

The energy is characterized by observing how fast the wall expands radially. The wall expansion as a function of time is measured by a streak camera, with an explosively-driven argon flash to back-light the tube. The film record is digitized to give radial expansion as a function of time. This curve is fit by the following analytic function, which is observed[14] to provide an excellent fit to expansion R[t] - R[0] versus time t:

$$R[t] - R[0] = (v_- \, t \, f[t])/((2v_-/a_0)f'[t] + f[t]) \quad (3)$$

where

$$f[t] = (1 + t)^n - 1 \quad (4)$$

where v_∞ is the asymptotic radial velocity and a_0 is the initial acceleration. At small expansions there is pronounced ringing of waves through the tube, but eqn. (3) is a smooth fit through these features. This is why a_0 in the fit is finite, whereas the actual initial acceleration is impulsive. For large expansions the internal pressure becomes small and the material "coasts". This is why the wall velocity approaches an asymptotic value v_∞. The fitting parameters are v_∞ = 1.6749 mm/μsec, a_0 = 0.8623 mm/μsec^2, and α = 0.9195 with R in mm and t in μs.

Differentiating eqn. (3) gives the radial velocity $v_r[t]$. This is plotted parametrically as a function of the radial tube expansion R[t] - R[0] in FIGURE 6. The figure of merit typically used to characterize the metal-pushing ability of an explosive is the so-called "cylinder energy", which is the quantity $0.5(v_t)^2$ evaluated at 19 mm radial expansion. The quantity $0.5(v_r)^2$ is close to, but not exactly, the kinetic energy per unit metal mass. For DAAF E_{19} = 1.22 kJ/g, which lies between that of PBX 9502 (1.04 kJ/g) and PBX 9501 (1.58 kJ/g).[7]

The detonation velocity was also measured via ten pin switches, each consisting of 2-mil diameter enamelled copper wire. When the detonation passes a wire, the insulation is promptly destroyed and the wire shorts to the tube. This fires an R-C circuit that is observed on an oscilloscope. The resulting detonation velocity was 8.020 mm/μs. The random error, i.e., the standard error in velocity associated with the linear fit to the x-t data, was 2.7 m/s.

FIGURE 6
Radial Velocity as a Function of Tube Expansion

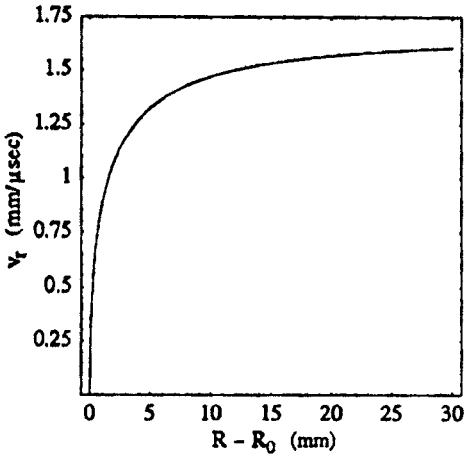

We were also interested in the related azo-compound DAAzF (3). Although it has less available oxygen it has a higher calculated ΔH_f (+146 kcal/mol). The thermal stability of (3) was also attractive having a DSC onset of 315°C, which is comparable to HNS. The published procedure[2] for preparing (3) only yielded inseparable mixtures as did the reduction of DAAF (2) with triphenylphosphine; therefore a new method of synthesizing (3) from readily available (2) was deduced via the intermediate hydrazine FIGURE 7.

This route also allowed us to examine the properties of the previously unknown hydrazine (6). Solid (6) very slowly oxidizes in air to (3); oxidation is more rapid in solution as it was efficiently converted to DAAzF (3) by bubbling air through a methanol solution. Interestingly, the ΔH_f of (6) was found to be only +50 kcal/mol. When compared to the ΔH_f of the azo-compound

FIGURE 7
Reduction of DAAF (2) to Hydrazine (6) and Oxidation to Azo-Compound (3)

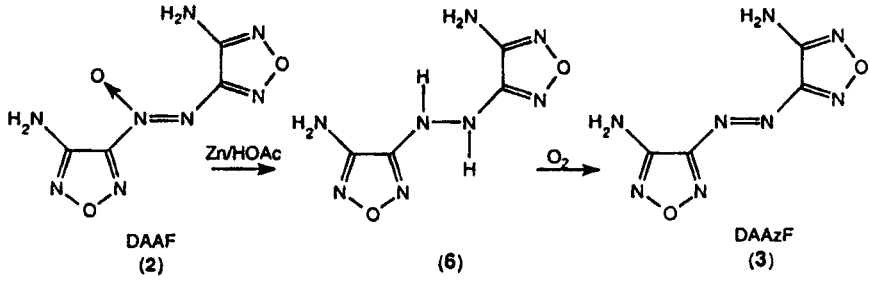

(3) (measured at +128 kcal/mol), and azoxy-compound (2) (measured at +106 kcal/mol), the amount of energy gained by having the azo- or azoxy- linkage in an energetic material can be observed. The azo-furazan (3) is a dark-orange crystalline solid which is insensitive to impact (H_{50}>320 cm, Type 12), spark (>0.36 J) and friction (>36 kg, BAM). A crystal density of 1.728 g/cm^3 was determined by x-ray.[8] The explosive performance of DAAzF (3) was lower in both velocity and pressure as the increase in heat of formation was not sufficient to offset the drop in oxygen balance compared to the azoxy-compound (2). This material was formulated with 5 vol.% latex Kel-F 800. The detonation velocity as a function of density was determined at two different diameters, 0.5 in. and 0.25 in. The velocity was more dependant on diameter than with DAAF (2) as shown in FIGURE 8. Despite this dependence a 3 mm diameter shot at a density of 1.65 g/cm^3 detonated cleanly with no confinement. A 0.5 in. diameter plate dent allowed the calculation of a detonation pressure to be 262 kbar at a density of 1.65 g/cm^3.

FIGURE 8
Detonation Velocity as a Function of Density at 0.5 in. and 0.25 in. for DAAzF (3) + 5 vol% Kel-F

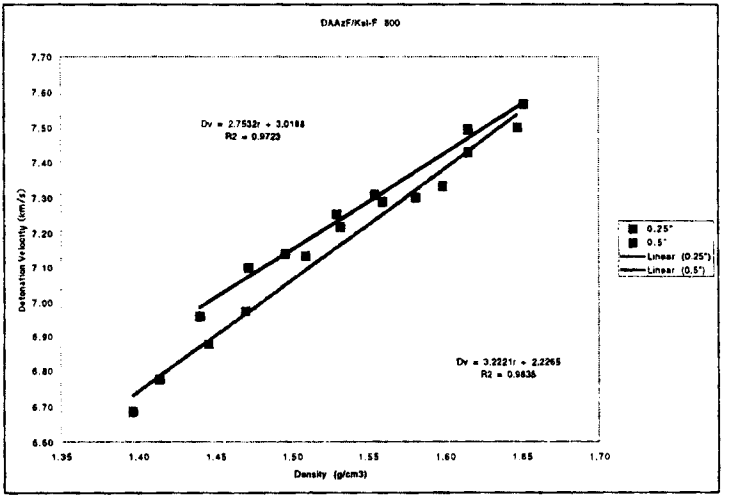

The final oxidation product investigated was the di-azo oxidation dimer DFT (4), FIGURE 9.

FIGURE 9
Preparation of bis[1,2,5]Oxadiazolo[3,4-c:3',4'-g][1,2,5,6]Tetrazocine

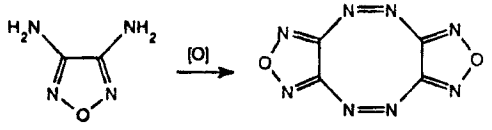

DAF (1) DFT (4)

This material had a predicted density of 1.91 g/cm^3 assuming the molecule to be planar and a calculated ΔH_f of +204 kcal/mol. Russian scientists claimed to have made this material in 1996 by

oxidizing DAF (1) with acetyl hypochlorite or sodium hypochlorite.[3] We attempted to prepare (4) by treating (1) with trichloroisocyanuric acid and obtained a product which did not match the properties reported by the Russians in melting point, ^{13}C NMR or IR. A crystal structure revealed that we had prepared the correct material and the molecule was in a boat configuration. This conformation severely depressed the density (1.758 g/cm^3)[8] when compared to the calculated planar, anti-aromatic structure. DFT (4) is a dangerous primary explosive with a drop height of approximately 4 cm (2.5 kg, Type 12, HMX=25 cm). We believe the sensitivity is due to the boat configuration as the azo-group's π-electrons are orthogonal to the π-electrons in the furazan rings, and thus no stabilization through delocalization can occur. One attempted oxidation of DFT (4) with peroxytrifluoroacetic acid yielded only a small amount of the azoxy-compound in admixture with the starting material as evidenced by ^{13}C NMR and was not further characterized.

EXPERIMENTAL

All starting materials were obtained from commercial sources or prepared from the referenced literature. All NMR spectra were obtained on a JEOL GSX-270 spectrometer, and chemical shifts are reported relative to internal tetramethylsilane. Elemental analyses were performed by W.F. King at Los Alamos National Laboratory. Melting points were determined at 2°C/min with a Mettler FP1 apparatus and are corrected or by Differential Scanning Calorimetry (DSC) at 2°C/min. IR spectra were obtained

on a Bio-Rad FTS-40 FTIR spectrometer. Poor agreement between theoretical and measured results in elemental analysis may be explained by the well known problem of microanalysis of high-nitrogen content compounds. However all compounds were purified to the point that agreement to at least two elements was within 0.4%.

3,3'-Diamino-4,4'-azoxyfurazan DAAF (2). This procedure was modeled from the original Russian preparation.[2] To 30% hydrogen peroxide (100.0 g, 0.88 mol) in a 500 ml jacketed flask maintained at 18°C was added 98% sulfuric acid (55.0 g, 0.56 mol) over 10 min. with stirring. The temperature was brought back down to 18°C and 3,4-diaminofurazan[3] (**1**) (10.0 g, 0.10 mol) was added. The suspension was stirred at 18°C for 24 hours in which time the soluble green nitroso-amino-furazan was converted to the insoluble orange DAAF. The product was filtered on a glass frit, washed with water and air dried to yield 9.29 g (88%) of crude material. For recrystallization the crude compound was dissolved in the minimum amount of room temperature DMSO (approximately 22 ml) and then water (45 ml) was added over 5 min. with stirring. The pure DAAF was filtered, washed with water and air-dried. This material was identical in all respects to that previously reported.[2] ^{1}H NMR (deuteriomethylsulfoxide)δ 6.65 (s, 2H), 6.93 (s, 2H); ^{13}C NMR (deuteriomethylsulfoxide)δ 148.3, 151.2, 152.6, 153.9.

3,3'-Diamino-4,4'-hydrazofurazan (6). A 1 l Erlenmeyer flask was charged with 200 ml of methanol, crude DAAF (**2**) (10.6 g, 0.050 mol) and zinc dust (9.77 g, 0.150 mol). To this

suspension was added glacial acetic acid (9.0 g, 0.150 mol) dropwise over 10 min. with good stirring. The slurry was stirred for 1 hour and then filtered through a bed of Celite. The bed was washed with methanol and the solvent removed under reduced pressure to yield 9.90 g (100%). An analytical sample was recrystallized from water to give a monohydrate, mp 192°C (dec.); ^{1}H NMR (deuteriomethylsulfoxide)δ 5.90 (s, 4H), 8.43 (s, 2H); ^{13}C NMR (deuteriomethylsulfoxide)δ 148.6, 150.3; IR (KBr) 3399, 3328, 3220, 3042, 1648, 1577, 1555, 1439, 1293, 913, 816 cm^{-1}.

Anal. Calcd for $C_4H_6N_8O_2 \cdot H_2O$: C, 22.23; H, 3.73; N, 51.87. Found: C, 22.03; H, 3.82; N, 52.27.

3,3'-Diamino-4,4'-azofurazan (3). Air was bubbled through the methanol solution of the hydrazo-furazan (**6**), prepared as above, for 20 hours with stirring at room temperature. The orange precipitate was filtered, washed with methanol and air dried to yield 9.0 g (92%) of pure (**3**) identical in all respects to that previously reported.[2] ^{1}H NMR (deuteriomethylsulfoxide)δ 6.89 (s, 4H); ^{13}C NMR (deuteriomethylsulfoxide)δ 150.4, 155.6.

Bis[1,2,5]oxadiazolo[3,4-c:3'4'-g][1,2,5,6]tetrazocine (4). To 50 ml of acetonitrile was added 3,4-diaminofurazan (1.0 g, 0.01 mol) with stirring until solution was complete. This solution was added dropwise to a solution of trichloroisocyanuric acid (4.65 g, 0.02 mol) in 50 ml of acetonitrile with stirring at room temperature over 15 min. The orange suspension was evaporated to dryness under reduced pressure and the remaining solid was extracted in a Soxhlet with hexane for 2 hours. The

hexane was removed under reduced pressure to yield 0.46 g (48%) of pure crystalline (**4**), mp 53.6°-54.5°C. ^{13}C NMR (deuterioacetone)δ 151.0; IR (KBr) 1545, 1190, 1168, 1025, 849, 724 cm^{-1}.

Anal. Calcd for $C_4N_8O_2$: C, 25.01; H, 0.00; N, 58.33. Found: C, 25.05; H, 0.13; N, 59.14.

REFERENCES

[1] M.D. Coburn, J. Heterocyclic Chem., **5**, 83 (1968).

[2] G.D. Solodyuk, M.D. Bolydrev, B.V. Gidaspov and V.D. Nikolaev, Zh. Org. Khim. **17**(4), 756 (1981) English Translation.

[3] L.V. Batog, L.S. Konstantinova, O.V. Lebedev and L.I. Khmel'nitskii, Mendeleev Commun., **5**, 193 (1996).

[4] V.E. Eman, M.S. Sukhanov, O.V. Lebedev, L.V. Batog, L.S. Konstantinova, V.Y. Rozhkov and L.I. Khmel'nitskii, Mendeleev Commun., **2**, 66 (1996).

[5] A. Gunasekaran, T. Jayachandran, J.H. Boyer and M.L. Trudell, J. Heterocyclic Chem., **32**(4), 1405 (1995).

[6] T.S. Novikova, T.M. Mel'nikova, O.V. Kharitonova, V.O. Kulagina, N.S. Aleksandrova, A.B. Sheremetev, T.S. Pivina, L.I. Khmel'nitskii and S.S. Novikov, Mendeleev Commun., **4**, 138 (1994).

[7] B.M. Dobratz, "Lawrence Livermore National Laboratory Explosives Handbook. Properties of Chemical Explosives and Explosives Simulants," National Technical Information Service, UCRL-52997, 1981.

[8] Density and structure determined by x-ray crystallography by R.D. Gilardi, Unpublished Results, Naval Research Laboratory,

Washington D.C.

[9] W.L. Seitz, Shock Waves in Condensed Matter, 531 (1983).

[10] L.G. Hill, W.L. Seitz, J.F. Kramer, D.M. Murk and R.S. Medina, Shock Compression of Condensed Matter, 803 (1995).

[11] T.R. Gibbs and A. Popolato, "Los Alamos Scientific Laboratory Explosives Property Data," University of California Press, 1980.

[12] J.J. Dick, C.A. Forest, J.B. Ramsay and W.L. Seitz, J. Appl. Phys., **63**(10), 4881 (1988).

[13] L.G. Hill and R.A. Catanach, Los Alamos Report LA-13442-MS (1998).

[14] L.G. Hill, Shock Waves, **1**, 355 (1997).